OPEN ACCESS
JOURNAL OF ADVANCED DIELECTRICS
Vol. 13, No. 5 (2023) 2350016 (8 pages)

DOI: 10.1142/S2010135X23500169

Achieving excellent temperature-stable dielectric properties of $Bi_{0.5}Na_{0.5}TiO_3$-based lead-free ceramics via doping $AgNbO_3$

Li-na Liu*, Xiao-ming Chen*,‡,¶, Xing-xing Wang* and Han-li Lian†,§,¶

*School of Physics and Information Technology, Shaanxi Normal University
Xi'an 710119, P. R. China

†School of Science, Xi'an University of Posts and Telecommunications
Xi'an 710121, P. R. China

‡xmchen@snnu.edu.cn

§lianhanli@163.com

Received 28 March 2023; Revised 5 May 2023; Accepted 9 May 2023; Published 31 May 2023

The lead-free ceramics $(1-x)(0.94Bi_{0.47}Na_{0.47}Ba_{0.06}TiO_3\text{-}0.06BiAlO_3)\text{-}xAgNbO_3$ (denoted as BNBTA-xAN) were synthesized via a solid-state sintering method. The effect of $AgNbO_3$ doping amount on dielectric properties of the ceramics was studied systematically. X-ray diffraction (XRD), scanning electron microscope (SEM) and Raman spectroscope were used to detect the structure of the ceramics. Temperature-dependent dielectric spectra, frequency-dependent dielectric constant and alternating current (ac) electric conductance at various temperatures were measured. The doping of $AgNbO_3$ greatly reduces dielectric constant around Curie temperature and thus enhances the temperature stability of the dielectric constant. The ceramic BNBTA-0.03AN exhibits excellent temperature-stable dielectric properties with temperature coefficient of capacitance (TCC) ≤±15% between 55°C and 418°C with temperature window 363°C and small changes of dielectric constant and dielectric loss from 100 Hz to 1 MHz at different temperatures. The obtained ceramics are expected to be used in high-temperature capacitors due to its excellent temperature stability.

Keywords: Microstructure; dielectric properties; lead-free ceramics; BNT.

1. Introduction

Dielectric capacitors are widely used in pulse power systems, electric vehicles, electronic components and so on. The operation temperatures of dielectric capacitors need to be higher than 200°C in fields such as deep-sea drilling, aerospace, nuclear industry and so on.[1,2] Large dielectric permittivity (ε_r) and temperature-stability of dielectric properties are equally important. In recent years, materials for capacitors including linear dielectrics such as TiO_2,[3] anti-ferroelectrics such as $AgNbO_3$,[4,5] lead-based ferroelectrics such as $Pb(Mg_{1/3}Nb_{2/3})O_3$ and $Pb(Zn_{1/3}Nb_{2/3})O_3$),[6,7] lead-free ferroelectrics such as $Bi_{0.5}Na_{0.5}TiO_3$-based ceramics[8–10] were extensively studied. Among these materials, $(1-x)$ $Bi_{0.5}Na_{0.5}TiO_3$-$xBaTiO_3$ with $x = 0.06$, i.e., $Bi_{0.47}Na_{0.47}Ba_{0.06}TiO_3$-based ceramics have attracted extensive attention. The composition of $Bi_{0.47}Na_{0.47}Ba_{0.06}TiO_3$ has a tetragonal rhombohedral morphotropic phase boundary (MPB).[11] The curves of the temperature-dependent ε_r always show two obvious dielectric anomalies, which are located around the temperatures denoted as T_{RE} and T_m.[12–15] At temperatures below T_{RE}, the ε_r values depend on frequency markedly. As temperature increases above T_{RE}, the ε_r values measured at different frequencies tend to merge together. At T_m, dielectric constant is the maximum (ε_m). The dielectric anomaly at T_{RE} is believed to be associated with the thermal evolution of R3c polar nanoregions (PNRs) and P4bm PNRs, and that at T_m is related to the transition between R3c and P4bm and the thermal evolution P4bm PNRs.[16] The reduction in the difference of ε_r between T_{RE} and T_m will facilitate improving temperature stability of dielectric constant. Furthermore, if the temperature span between T_{RE} and T_m can be widened, it is expected to obtain materials for high-temperature capacitors used in a wide temperature window. Temperature coefficient of capacitance (TCC) is always used to characterize temperature stability of ε_r:

$$\mathrm{TCC} = (C_T - C_{150})/C_{150}, \tag{1}$$

where C_T is capacitance at temperature T, and C_{150} is capacitance at 150°C.[17] Wider temperature range of TCC ≤ ±15% means better temperature stability of ε_r.

As a lead-free anti-ferroelectric, $AgNbO_3$ has been used to improve dielectric properties of $Bi_{0.5}Na_{0.5}TiO_3$-based ceramics.[18–20] Ren *et al*. found that the incorporation of $AgNbO_3$ into $(Bi_{0.5}Na_{0.5})_{0.94}Ba_{0.06}TiO_3$ shifts the temperature of transition from low symmetry PNRs to higher symmetry ones to room temperature and the temperature range

¶Corresponding authors.

between the two dielectric anomalies widens.[19] Wang *et al*. reported that the doping of a small amount of $AgNbO_3$ into $[(Bi_{0.55}Na_{0.45})_{0.94}Ba_{0.06}]_{0.98}La_{0.02}TiO_3$ broadens the dielectric-temperature plateau between the two anomalies.[20] Zheng *et al*. reported that the ceramic $(1-x)(Bi_{0.5}Na_{0.5})_{0.94}Ba_{0.06}TiO_3$-$xAgNbO_3$ with $x = 0.05$ exhibits excellent temperature-stable permittivity with the broad temperature range of TCC≤ ±15% between 40°C and 387°C.[18] The reports show that temperature-dependent dielectric properties of $Bi_{0.5}Na_{0.5}TiO_3$-based ceramics can be tuned by the doping of $AgNbO_3$. However, the temperature on the high-temperature side of TCC≤ ±15% is still less than 400°C in these studies.

In our previous work,[21,22] it was found that the addition of $BiAlO_3$ into $Bi_{0.5}Na_{0.5}TiO_3$-based ceramics can reduce the difference in ε_r between the two dielectric anomalies and broaden the temperature range between T_{RE} and T_m. Here, based on the previous work, $AgNbO_3$ was further doped into $0.94Bi_{0.47}Na_{0.47}Ba_{0.06}TiO_3$-$0.06BiAlO_3$ to achieve excellent temperature-stable dielectric constant. The effect of $AgNbO_3$ doping on phase structure, microstructure and temperature-dependent dielectric properties of the ceramics were systematically investigated. The results show that the ceramic with $x = 0.03$ exhibits excellent temperature-stable dielectric constant with TCC ≤ ±15% between 55°C and 418°C, which can be used in high temperature capacitors.

2. Experimental Procedures

$(1-x)(0.94Bi_{0.47}Na_{0.47}Ba_{0.06}TiO_3$-$0.06BiAlO_3)$-$xAgNbO_3$ (abbreviated as BNBTA-xAN, x = 0, 0.01, 0.03 and 0.05) lead-free ceramics were fabricated by means of a conventional solid-state sintering method. The raw materials $BaCO_3$ (purity ≥ 99.0%), TiO_2 (purity ≥ 98.0%), Bi_2O_3 (purity ≥ 98.9%), Na_2CO_3 (purity ≥ 99.8%), Al_2O_3 (purity ≥ 99.99%), Nb_2O_5 (purity ≥ 99.5%) and Ag_2O (purity ≥ 99.7%) were baked for 24 h at 120°C, and then weighted in a stoichiometric ratio. The powders with the given compositions were ball milled for 24 h and then dried. The dried powders were first calcined at 900°C for 3 h, and then ball milled with alcohol for 12 h. The obtained powders were then pressed into pellets with a diameter of 10 mm and a thickness of about 1 mm. Finally, the pellets were sintered at 1150°C for 2 h in an oxygen atmosphere.

Crystallite structure of the ceramics was analyzed by means of X-ray diffraction (XRD) instrument (D/Max2550, Rigaku, Japan) with Cu K_α radiation. The working voltage and current are 40 kV and 100 mA, respectively. *In-situ* XRD measurement was carried out at temperatures between room temperature and 500°C. Bulk density of the ceramics was measured according to the Archimedes method. Microstructure of the ceramics was observed via a scanning electron microscope (Nova Nano SEM 450, FEI, American) after being polished and thermally etched at 1050°C for one hour. An Almega-TM laser Raman spectrometer produced by Therm Nicolet was used for measuring Raman spectra. The samples were polished, cleaned and then covered the two surfaces with silver electrodes for measuring dielectric properties. Dielectric properties and alternating current (ac) electric conductance were measured on Agilent E4980A LCR meter.

3. Results and Discussion

Figure 1(a) shows the XRD curves of the BNBTA-xAN ceramics measured at room temperature. All samples present a pure perovskite structure without any secondary phase. All peaks are well indexed according to JCPDS No. 89-3109,[23] indicating pseudo-cubic phase. Figure 1(b) shows a magnified view of the peak (110). It is found that the peak of the ceramics with doping $AgNbO_3$ shifts towards higher angle direction compared to that of the ceramics with $x = 0$, indicating lattice shrinkage due to the doping and confirming entrance of the dopants into the crystallite lattice. The structure refinement was carried out based on the pseudo-cubic phase by means of the software Jade 6.0[24] and the obtained lattice parameters are shown in Table 1. The lattice constant (a) and lattice volume (V) change with increasing x. The ceramics with doping $AgNbO_3$ exhibit lower a and V values compared to the ceramic without doping. With an increase of x from 0.01 to 0.05, the changes in a and V are not monotonous and the ceramic with $x = 0.03$ exhibits a slight increase in a and V. According to the ionic radii given by Shannon,[25] the radius of Ag^+ is 1.53 Å in the case of coordination number (CN) = 12 and 1.15 Å for CN = 6, that of Nb^{5+} is 0.69 Å for CN = 12 and 0.64 Å for CN = 6, and the ionic radii of Ba^{2+} and Na^+ with

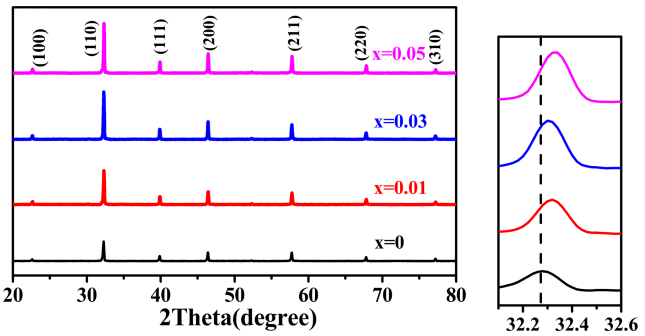

(a) (b)

Fig. 1. XRD curves of the ceramics at room temperature (a) and the magnified view of the (110) peak (b).

Table 1. Lattice parameters and lattice volume of the ceramics.

Samples	Lattice constant a (Å)	Lattice volume V (Å^3)
$x = 0$	3.909(3)	59.742(1)
$x = 0.01$	3.907(4)	59.658(2)
$x = 0.03$	3.908(7)	59.716(9)
$x = 0.05$	3.906(3)	59.607(8)

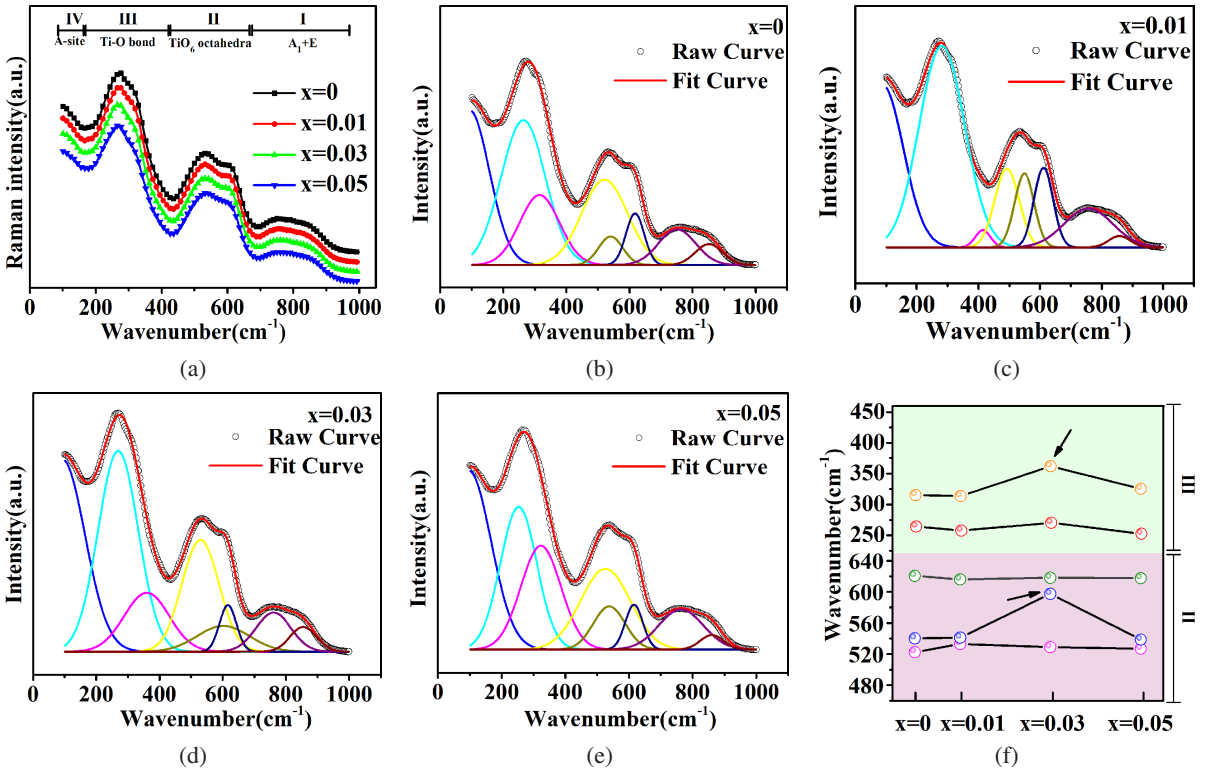

Fig. 2. (a) Raman spectroscopy of the ceramics at room temperature, (b)–(e) fitting curves of Raman spectroscopy according to the Gauss-Boltzmann modes and (f) typical positions of Raman vibration modes.

CN = 12 are 1.61 Å and 1.39 Å, respectively. The ionic radius of Bi^{3+} with CN = 12 was calculated to be 1.36 Å by extrapolation method, since it is not available in Shannon's table.[11] So, Ag^{+} and Nb^{5+} should enter into the A-site and B-site, respectively. For $0.94Bi_{0.47}Na_{0.47}Ba_{0.06}TiO_3$-$0.06BiAlO_3$, the average size of the cations in the A-site is 1.089 Å and the average size of the cations in the B-site is 0.821 Å. The radius of Ag^{+} is larger than the mean size of the cations in the A-site, while that of Nb^{5+} is smaller than the mean size of the B-site cations. Besides, the electric charge of Nb^{5+} is different from that of Ti^{4+} and Al^{3+} in the B-site, and the electric charge of Ag^{+} is different from that of Bi^{3+} and Ba^{2+} in the A-site. The substitution of cations with different electric charges will introduce point defects in the samples,[26] which should also influence lattice distortion. It is expected that the competition effects mentioned above cause the change in lattice constant.

Figure 2(a) shows the Raman spectra of the ceramics. There are four regions on the spectra. Region I with wavenumber $\lambda^{-1} > 700$ cm^{-1} is related to the longitudinal optical modes A and E. In Region II (450 cm^{-1} < λ^{-1} < 700 cm^{-1}), the peaks are associated with the vibration of TiO_6 octahedron. The peaks in Region III (around 250 cm^{-1}) are associated with the vibration of Ti–O bond. Region IV is related to the vibration of cations in the A-site. The Raman spectra were fitted using Gauss–Boltzmann curves by means of the software Origin.[27] The fitting results are displayed in Figs. 2(b)–2(e). The peak positions in Region II corresponding to TiO_6 octahedron and in Region III corresponding to Ti–O bond are shown in Fig. 2(f). It is found that the peak positions change with an increase in x and the ceramic with x = 0.03 shows increased wavenumbers (Fig. 2(f)). The changes in Raman spectra further confirm the lattice distortion due to the doping of $AgNbO_3$.

The Archimedes method is used to measure bulk density (ρ_b) of the ceramics. Theoretical density (ρ_{th}) was calculated according to the formula of $\rho_{th}=M\times Z/(6.02\times10^{23}\times V)$, in which M is the molecular mass, V is the lattice volume and Z is the subcell number. Relative density (ρ_r) was obtained via the formula of $\rho_r=\rho_b/\rho_{th}\times100\%$. Changes of ρ_b, ρ_{th} and ρ_r of the ceramics as a function of x are shown in Fig. 3. With the increase of x, the bulk density increases from 5.84 g/cm^3 for x = 0 to 6.01 g/cm^3 for x = 0.05. The theoretical density changes slightly from 6.10 g/cm^3 to 6.11 g/cm^3 as x increases from 0 to 0.05. The relative densities of all ceramics are higher than 95%, and the ceramics with x = 0.03 and 0.05 show ρ_r values larger than 97%, suggesting the ceramics were well sintered. Figure 4 shows SEM images of the ceramics. All ceramics show dense microstructures, which corresponds to their high relative densities. The distribution of grain size was obtained via the software of Nano Measure and the mean grain sizes were calculated, as demonstrated in the insets of Fig. 4. The ceramics with different x have the average grain sizes around 1.0 μm.

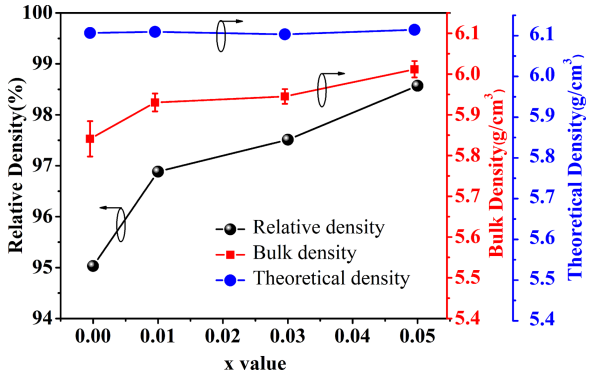

Fig. 3. Bulk density, theoretical density and relative density of the ceramics.

Variation in dielectric constant (ε_r) and dielectric loss (tanδ) of the ceramics as a function of temperature is shown in Fig. 5. There are two obvious abnormal dielectric peaks, which are similar to other $Bi_{0.5}Na_{0.5}TiO_3$-based ceramics.[28–30] The first dielectric anomaly is at the temperature denoted as T_{RE}. At T_{RE}, the dielectric constant (ε_{RE}) at different frequencies merges together. The second dielectric anomaly locates at the temperature denoted as T_m. The T_m is determined as the temperature at which the dielectric constant approaches the maximum (ε_m). The values of T_{RE}, T_m, ε_{RE}, ε_m are shown in Table 2. For a given sample, when the temperature is between T_{RE} and T_m, the ε_r values are almost unchanged with increasing temperature, and the frequency dispersion disappears, exhibiting excellent temperature and frequency-stability of ε_r.

TCC is one of the important parameters for characterizing temperature-stable dielectric properties for capacitor materials. The temperature-dependent dielectric spectrum at 1 kHz is shown in the inset of Fig. 6, and the calculated TCC curves of the ceramics at 1 kHz between 25°C and 450°C are shown in Fig. 6. As can be seen, the different $AgNbO_3$ amounts cause change in TCC curves. The values of ε_r,150°C, temperature range for TCC ≤ 15%, and temperature window for TCC ≤ 15% (ΔT) are shown in Table 3. The temperature stability of dielectric constant is enhanced by the doping of $AgNbO_3$. The ceramic with $x = 0$ shows the temperature window of 182°C for TCC ≤ 15% between 100°C and 282°C, while all doped ceramics exhibit the temperature windows higher than 300°C. Especially, the sample with $x = 0.03$ shows the highest temperature window of 363°C for TCC ≤ 15% between 55°C and 418°C. The temperature on the high-temperature side of TCC≤ ±15% has been higher than 400°C. The temperature stability properties of the present $AgNbO_3$-doped $0.94Bi_{0.47}Na_{0.47}Ba_{0.06}TiO_3$-$0.06BiAlO_3$ ceramics (i.e., BNBTA-xAN) are also compared with those of the $NaNbO_3$-doped $0.94Bi_{0.47}Na_{0.47}Ba_{0.06}TiO_3$-$0.06BiAlO_3$ ceramics (i.e., BNBTA-xNN) reported in our previous work in Table 3. The BNBTA-xNN ceramics show the ΔT values lower than 300°C.[28] The ε_r values at 150°C, temperature range for TCC ≤ ±15%, and temperature window (ΔT) of BNT-based ceramics reported by others are also compared in Table 3. The comparison shows that via doping $AgNbO_3$, more excellent

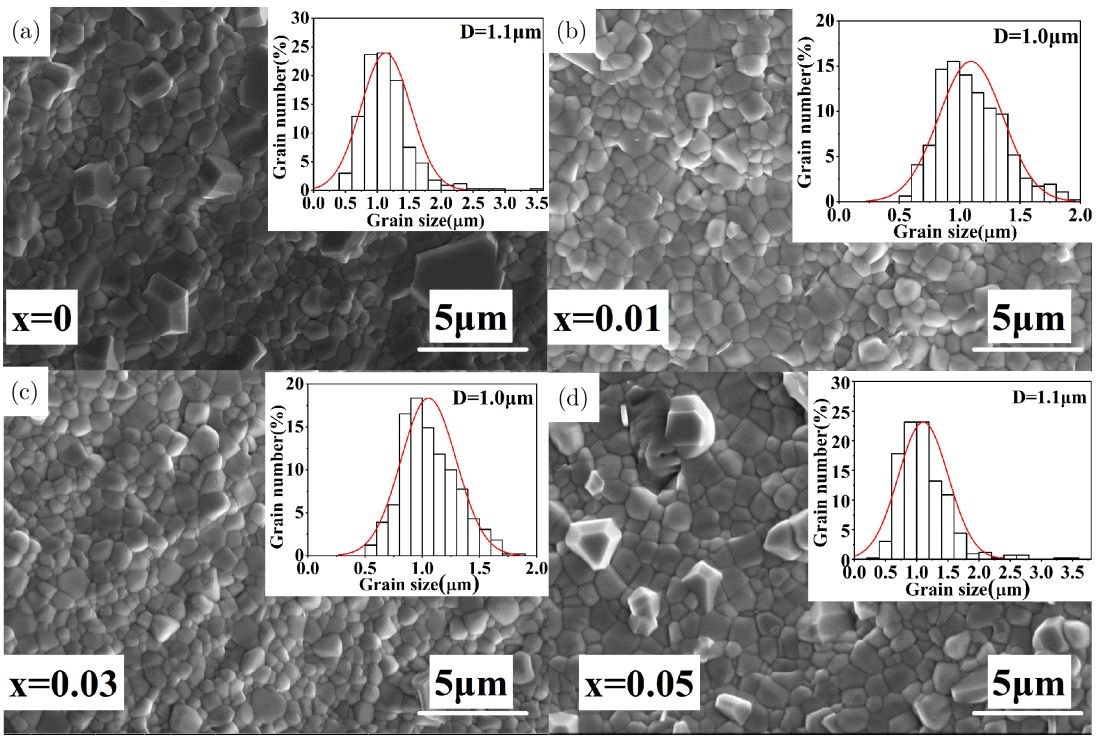

Fig. 4. SEM images of the fractured surfaces of the ceramics. The insets show size distribution of grains in the ceramics.

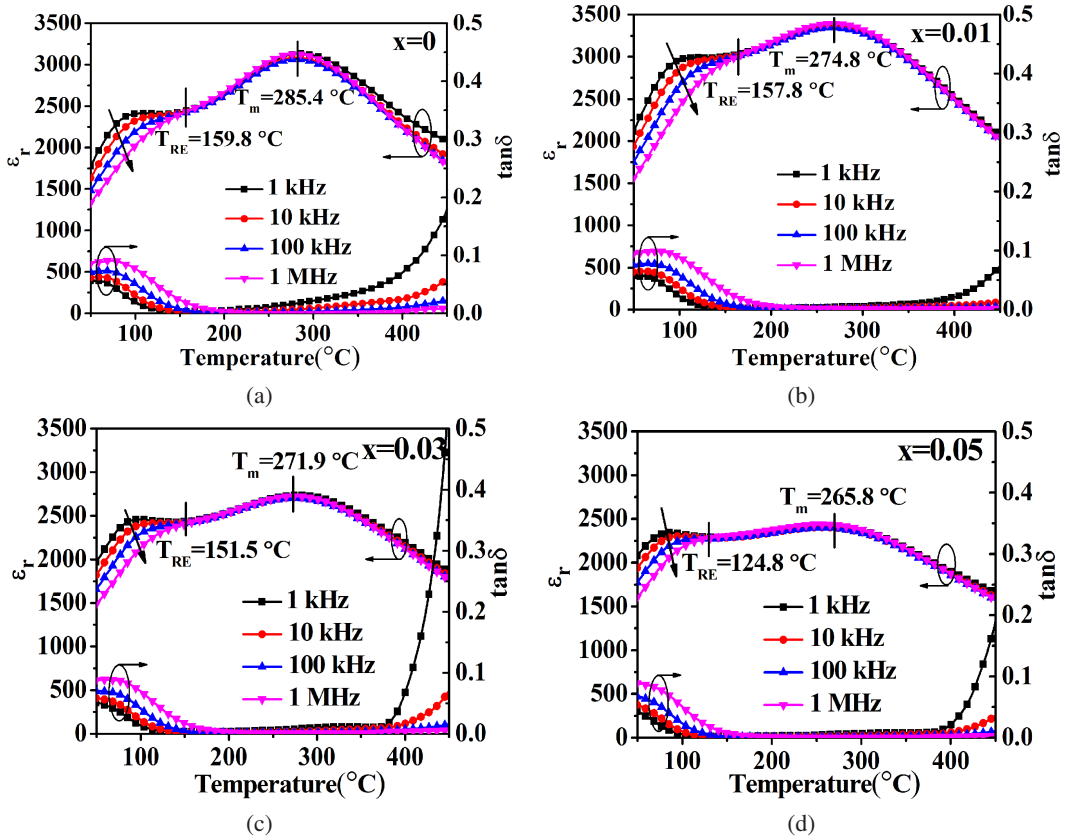

Fig. 5. Dielectric constant (ε_r) and dielectric loss (tanδ) of the ceramics versus temperature at different frequencies.

Table 2. Values of T_{RE}, T_m, ε_{RE} and ε_m of the ceramics measured at 1 kHz.

Samples	T_{RE} (°C)	T_m (°C)	ε_{RE}	ε_m
x = 0	159.8	285.4	2442	3132
x = 0.01	157.8	274.8	3035	3370
x = 0.03	151.5	271.9	2433	2734
x = 0.05	124.8	265.8	2290	2417

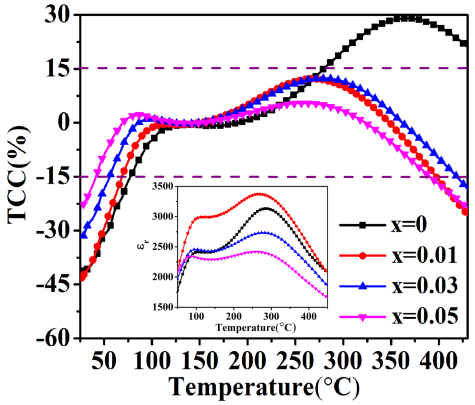

Fig. 6. Temperature dependence of TCC for the ceramics in the temperature range between 25°C and 450°C. The temperature-dependent dielectric spectrum at 1 kHz is shown in the inset.

Table 3. Comparison of temperature stability of ε_r for various BNT-based ceramics.

Samples	ε_r (150°C, 1 kHz)	Temperature range for T_{CC}≤15% (°C)	Temperature window for T_{CC}≤15% (ΔT) (°C)	Ref.
BNBTA-0AN	2427	100–282	182	This work
BNBTA-0.01AN	3006	69–395	326	This work
BNBTA-0.03AN	2433	55–418	363	This work
BNBTA-0.05AN	2291	40–389	349	This work
BNBTA-0NN	3042	66–231	165	28
BNBTA-0.01NN	2887	66–266	200	28
BNBTA-0.03NN	2982	78–354	276	28
BNBTA-0.05NN	2688	58–344	286	28
BNST-7.5BS	2081	43–255	212	31
BNTBT-5AN	2329	40–387	347	18
0.8BNT-0.2PMN	3300	56–350	294	32
BNT-BT-10NBN	1988	25–337	312	33

The abbreviation for the samples' name is as follows:
BNBTA-xNN: $(1-x)(0.94Bi_{0.47}Na_{0.47}Ba_{0.06}TiO_3$-$0.06BiAlO_3)$-$xNaNbO_3$ with x = 0, 0.01, 0.03 and 0.05.
BNST-7.5BS: $0.975Bi_{0.38}Na_{0.38}Sr_{0.24}TiO_3$-$0.025BaSnO_3$,
BNTBT-5AN: $0.95[(Bi_{0.5}Na_{0.5})_{0.94}Ba_{0.06}TiO_3]$-$0.05AgNbO_3$,
0.8BNT-0.2PMN: $0.8Bi_{1/2}Na_{1/2}TiO_3$-$0.2PbMg_{1/3}Nb_{2/3}O_3$,
BNT-BT-10NBN: $0.9(0.94Na_{0.5}Bi_{0.5}TiO_3$-$0.06BaTiO_3)$-$0.1Na_{0.73}Bi_{0.09}NbO_3$.

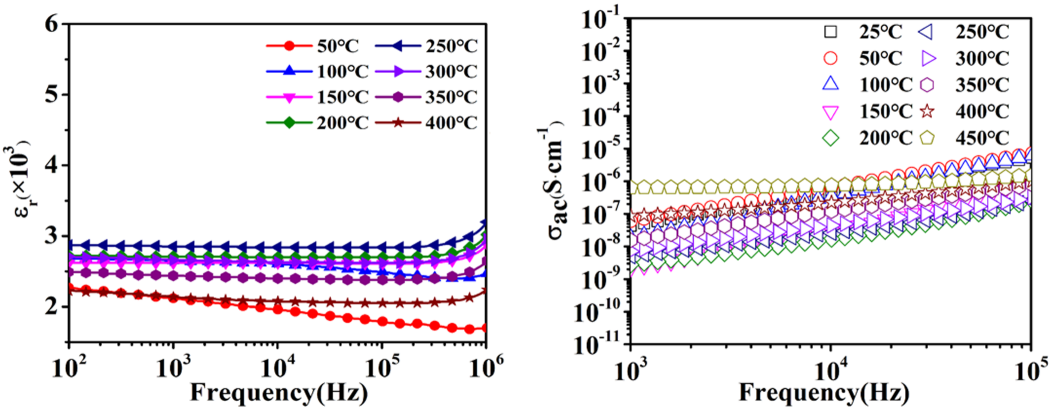

(a) (b)

Fig. 7. Changes of ε_r (a) and ac conductance σ_{ac} (b) as a function of frequency at different temperatures for the ceramic with $x = 0.03$.

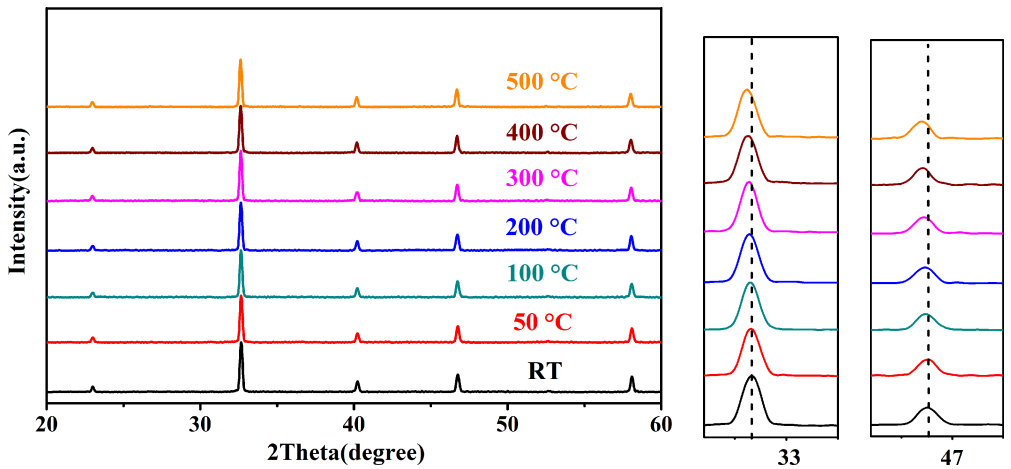

(a) (b) (c)

Fig. 8. *In-situ* temperature XRD curves of the ceramic with $x = 0.03$ measured at temperatures between room temperature and (a) 500°C, (b) magnified view of the peaks around 33° and (c) 47°.

temperature stability of dielectric constant with TCC ≤ 15% between 55°C and 418°C is obtained.

Changes of ε_r as a function of frequency at different temperatures for the sample with $x = 0.03$ are shown in Fig. 7(a). In the temperature range between 50°C and 400°C, ε_r increases first and then decreases between 100 Hz and 1 MHz, reaching its maximum value at 250°C. The changes of ε_r at different temperatures are the same as the results of dielectric spectrum as a function of temperature (Fig. 5). Figure 7(b) shows the changes of ac electric conductance as a function of frequency measured at temperatures between 25°C and 400°C for the ceramic with $x = 0.03$. For a given temperature, the conductance increases with an increase in frequency. The ceramic with $x = 0.03$ maintains conductivity lower than 10^{-5} S•cm^{-1} at all measuring frequencies and temperatures. The frequency-dependent dielectric spectrum and frequency-dependent conductance spectrum at various temperatures reflect good dielectric temperature stability.

To further explore the temperature stability, *in-situ* temperature XRD measurement was carried out for the ceramic with $x = 0.03$ and the result is shown in Fig. 8. As can be seen, the peaks shift towards lower 2 theta direction with increasing temperature, reflecting lattice expansion due to the increased temperature. No peak was found to be split during the measurement temperature range within the XRD detection precision limit, suggesting that the sample keeps a pseudo-cubic structure between the room temperature and 500°C which facilitates temperature-stable dielectric properties.

4. Conclusions

The lead-free ceramics BNBTA-*x*AN with dense microstructures were prepared via a solid-state sintering method. All samples have pure perovskite structure. The $AgNbO_3$-doped ceramics exhibit widened temperature window for TCC ≤ ±15% compared to the ceramic without doping. The ceramic

with $x = 0.03$ demonstrates excellent temperature stability of ε_r with TCC ≤ 15% between 55°C and 418°C with a temperature window of 363°C. At the same time, the sample with $x = 0.03$ exhibits small changes in ε_r and tanδ from 100 Hz to 1 MHz at different temperatures. Via doping $AgNbO_3$, excellent temperature-stable dielectric properties of $Bi_{0.5}Na_{0.5}TiO_3$-based ceramics were achieved, making hopeful application in high-temperature capacitors.

Acknowledgments

This work was supported by the National Natural Science Foundation of China (Nos. 52272118 and 51972202) and Shaanxi Province Science and Technology Foundation (No. 2022JM022).

References

[1]X. M. Chen, H. Y. Ma, W. Ding, Y. Zhang, X. G. Zhao, X. Liang and P. Liu, Microstructure, dielectric, and piezoelectric properties of $Pb_{0.92}Ba_{0.08}Nb_2O_6$-0.25wt% TiO_2 ceramics: Effect of sintering temperature, *J. Am. Ceram. Soc*. **94**, 3364 (2011).

[2]W. T. Chen, A. E. Gurdal, S. Tuncdemir, J. Gambal, X. M. Chen and C. A. Randall, Introducing an extremely high output power and high temperature piezoelectric bimorph energy harvester technology based on the ferroelectric system $Bi(Me)O_3$-$PbTiO_3$, *J. Appl. Phys*. **128**, 144102 (2020).

[3]H. Usui, K. Koseki, T. Tamura, Y. Domi and H. Sakaguchi, Light energy storage in TiO_2/MnO_2 composite electrode for photoelectron chemical capacitor, *Mater. Lett*. **186**, 338 (2017).

[4]Y. L. Zhang, X. B. Li, J. M. Song, S. W. Zhang, J. Wang, X. H. Dai, B. T. Liu, G. Y. Dong and L. Zhao, $AgNbO_3$ antiferroelectric film with high energy storage performance, *J. Materiomics* **7**, 1294 (2021).

[5]J. Li, Y. Tian, Y. Lan, L. Jin, C. Chen and X. Y. Wei, Silver deficiency effect on dielectric properties and energy storage performance of $AgNbO_3$ ceramics, *Ceram. Int.* **47**, 26178 (2021).

[6]T. F. Zhang, X. G. Tang, Q. X. Liu, Y. P. Jiang, X. X. Huang and Q. F. Zhou, Energy-storage properties and high-temperature dielectric relaxation behaviors of relaxor ferroelectric $Pb(Mg_{1/3}Nb_{2/3})O_3$-$PbTiO_3$ ceramics, *J. Phys. D. Appl. Phys*. **49**, 95302 (2016).

[7]Q. Gao, Q. Y. Hu, L. Jin, M. V. Gorev, D. S. Chezganov, E. O. Vlasov, H. R. Zeng, L. Y. Zhao, Y. Cui, Z. Xu and X. Y. Wei, Dielectric relaxation and phase transition behavior of (1−x) $Pb(Zn_{1/3}Nb_{2/3})O_3$-$xBaTiO_3$ binary solid solutions, *Ceram. Int*. **44**, 18491 (2018).

[8]X. Y. Zhao, W. F. Bai, Y. Q. Ding, L. J. Wang, S. T. Wu, P. Zheng P. Li and J. W. Zhai, Tailoring high energy density with superior stability under low electric field in novel $(Bi_{0.5}Na_{0.5})TiO_3$-based relaxor ferroelectric ceramics, *J. Eur. Ceram. Soc*. **40**, 4475 (2020).

[9]D. X. Li, Z. Y. Shen, Z. P. Li, W. Q. Luo, X. C. Wang, Z. M. Wang, F. S. Song and Y. M. Li, P-E hysteresis loop going slim in $Ba_{0.3}Sr_{0.7}$-TiO_3-modified $Bi_{0.5}Na_{0.5}TiO_3$ ceramics for energy storage applications, *J. Adv. Ceram*. **9**, 183 (2020).

[10]Q. Li, J. Wang, Y. Ma, L. T. Ma, G. Z. Dong and H. Q. Fan, Enhanced energy-storage performance and dielectric characterization of $0.94Bi_{0.5}Na_{0.5}TiO_3$-$0.06BaTiO_3$ modified by $CaZrO_3$, *J. Alloys Compd*. **663**, 701 (2016).

[11]T. Takenaka, K. Maruyama and K. Sakata, $(Bi_{1/2}Na_{1/2})TiO_3$-$BaTiO_3$ system for lead-free piezoelectric ceramics, *Jpn. J. Appl. Phys*. **30**, 2236 (1991).

[12]X. S. Qiao, X. M. Chen, H. L. Lian, W. T. Chen, J. P. Zhou and P. Liu, Microstructure and electrical properties of nonstoichiometric $0.94(Na_{0.5}Bi_{0.5+x})TiO_3$-$0.06BaTiO_3$ lead-free ceramics, *J. Am. Ceram. Soc*. **99**, 198 (2016).

[13]X. S. Qiao, X. M. Chen, H. L. Lian, J. P. Zhou and P. Liu, Dielectric, ferroelectric, piezoelectric properties and impedance analysis of nonstoichiometric $(Bi_{0.5}Na_{0.5})_{0.94+x}Ba_{0.06}TiO_3$ ceramics, *J. Eur. Ceram. Soc*. **36**, 3995 (2016).

[14]R. Y. Jing, X. M. Chen, H. L. Lian, X. S. Qiao, X. J. Shao and J. P. Zhou, Comparative study on structure, dielectric, and piezoelectric properties of $(Na_{0.47}Bi_{0.47}Ba_{0.06})_{0.95}A0.05TiO_3$ (A = Ca^{2+}/Sr^{2+}) ceramics: Effect of radii of A-site cations, *J. Eur. Ceram. Soc*. **38**, 3111 (2018).

[15]H. L. Lian, X. J. Shao and X. M. Chen, Structure and electrical properties of Ca^{2+}-doped $(Na_{0.47}Bi_{0.47}Ba_{0.06})TiO_3$ lead-free piezoelectric ceramics, *Ceram. Int*. **44**, 11320 (2018).

[16]W. Jo, S. Schaab, E. Sapper, L. A. Schmitt, H. J. Kleebe, A. J. Bell and J. Rodel, On the phase identity and its thermal evolution of lead free $(Bi_{1/2}Na_{1/2})TiO_3$-6 mol% $BaTiO_3$, *J. Appl. Phys*. **110**, 074106 (2011).

[17]Y. H. Wan, L. Tang, X. Y. Dang, P. R. Ren, M. Ma, K. X. Song and G. Y. Zhao, High temperature dielectrics based on $Bi_{1/2}Na_{1/2}$-TiO_3-$BaTiO_3$-$Sr_{0.53}Ba_{0.47}Nb_2O_6$ ceramics with high dielectric permittivity and wide operational temperature range, *Ceram. Int*. **45**, 2596 (2019).

[18]S. Q. Zheng, Q. Li, Y. Q. Chen, A. K. Yadav, W. J. Wang and H. Q. Fan, Enhanced energy storage density with excellent temperature-stable dielectric properties of $(1 - x)[(Bi_{0.5}Na_{0.5})_{0.94}Ba_{0.06}TiO_3]$-$xAgNbO_3$ lead-free ceramics, *J. Alloys Compd*. **911**, 165019 (2022).

[19]P. R. Ren, Z. C. Liu, H. Liu, S. D. Sun, Y. H. Wan, C. B. Long, J. Shi, J Chen and G. Y. Zhao, Large electrostrain and structural evolution in $(1 - x)[0.94Bi_{0.5}Na_{0.5}TiO_3$-$0.06BaTiO_3]$-$xAgNbO_3$ ceramics, *J. Eur. Ceram. Soc*. **39**, 994 (2019).

[20]H. Wang, X. L. Jang, X. Q. Liu, R. N. Yang, Y. Yang, Q. J. Zheng, K. W. Kwok and D. M. Lin, An effective approach to achieve high energy storage density and efficiency in BNT-based ceramics by doping $AgNbO_3$, *Dalton Trans*. **48**, 17864 (2019).

[21]J. Wang, X. M. Chen, X. M. Zhao, X. X. Liang, J. P. Zhou and P. Liu, Effects of $BiAlO_3$-doping on dielectric and ferroelectric properties of $0.93Na_{0.5}Bi_{0.5}TiO_3$-$0.07BaTiO_3$ lead-free ceramics, *Mater. Res. Bull*. **67**, 94 (2015).

[22]Y. Z. Qiu, X. M. Chen, H. L. Lian, J. P. Ma and W. Q. Ouyang, Structure and electrical behavior of unpoled and poled $0.97(Bi_{0.5}$-$Na_{0.5})_{0.94}Ba_{0.06}TiO_3$-$0.03BiAlO_3$ ceramics, *Mater. Chem. Phys*. **202**, 197 (2017).

[23]X. Liu, X. M. Chen, L. N. Liu and G. B. Zhang, Effect of $BiAlO_3$ doping on dielectric and ferroelectric properties of $(Bi_{0.5}$-$Na_{0.42}K_{0.08})_{0.96}Sr_{0.04}Ti_{0.975}Nb_{0.025}O_3$ lead-free ceramics, *J. Mater. Sci. Mater. Electron* **31**, 17491 (2020).

[24]R. Y. Jing, X. M. Chen, J. P. Ma, H. L. Lian and W. T. Chen, Synthesis, microstructure, and electrical behavior of $(Na_{0.5}Bi_{0.5})_{0.94}Ba_{0.06}$-$TiO_3$ piezoelectric ceramics via a citric acid sol-gel method, *J. Mater. Sci*. **53**, 274 (2018).

[25]R. D. Shannon, Revised effective ionic radii and systematic studies of interatomic distances in halides and Chalcogenides, *Acta Cryst. A* **32**, 751 (1976).

[26]X. M. Chen, L. N. Liu, X. X. Wang and M. D Liu, An overview of structure and electrical properties of $(Na_{0.5}Bi_{0.5})_{0.94}Ba_{0.06}TiO_3$ ceramics: Point defects effect, *J. Shaanxi Normal Univ. (Nat. Sci. Ed.)* **49**, 1 (2021).

[27]A. Prado, L. Ramajo, J. Camargo, A. D. Campo, P. Öchsner, F. Rubio-Marcos and M. Castro, Stabilization of the morphotropic phase boundary in $(1-x)Bi_{0.5}Na_{0.5}TiO_3$-$xBaTiO_3$ ceramics through two alternative synthesis pathways, *J. Mater. Sci. Mater. Electron*. **30**, 18405 (2019).

[28]L. N. Liu, X. M. Chen, H. L. Lian, X. X. Wang, J. B. Lu, X. Liu, J. P. Zhou and P. Liu, Temperature-stable dielectric and energy storage properties of $(0.94Bi_{0.47}Na_{0.47}Ba_{0.06}TiO_3$-$0.06BiAlO_3)$-$NaNbO_3$ ceramics, *J. Alloys Compd*. **847**, 156409 (2020).

[29]X. M. Zhao, X. M. Chen, J. Wang, X. X. Liang, J. P. Zhou and P. Liu, Effects of Ti nonstoichiometry on microstructure, dielectric, ferroelectric and piezoelectric properties of $(Na_{0.54}Bi_{0.5})_{0.94}Ba_{0.06}Ti_{1+x}O_3$ lead-free ceramics, *J. Ceram. Process. Res*. **16**, 18 (2015).

[30]S. Prasertpalichat, S. Khengkhatkan, T. Siritanon, J. Jutimoosik, P. Kidkhunthod, T. Bongkarn and E. A. Patterson, Comparison of structural, ferroelectric, and piezoelectric properties between A-site and B-site acceptor doped $0.93Bi_{0.5}Na_{0.5}TiO_3$-$0.07BaTiO_3$ lead-free piezoceramics, *J. Eur. Ceram. Soc*. **41**, 4116 (2021).

[31]F. Yang, H. Wang, Q. Li, A. K. Yadav and H. Q. Fan, High energy storage density and temperature-stable dielectric properties for $(1 - x)Bi_{0.38}Na_{0.38}Sr_{0.24}TiO_3$-$xBaSnO_3$ lead-free relaxor ceramics, *Ceram. Int*. **47**, 33162 (2021).

[32]F. T. Hu, X. F. Chen, P. Peng, F. Cao, X. L. Dong and G. S. Wang, High permittivity $(1 - x)Bi_{1/2}Na_{1/2}TiO_3$-$xPbMg_{1/3}Nb_{2/3}O_3$ ceramics for high-temperature-stable capacitors, *J. Am. Ceram. Soc*. **101**, 4434 (2018).

[33]J. B. Wang, H. Q. Fan, B. Hu and H. Jiang, Enhanced energy-storage performance and temperature-stable dielectric properties of $(1 - x)(0.94Na_{0.5}Bi_{0.5}TiO_3$-$0.06BaTiO_3)$-$xNa_{0.73}Bi_{0.09}NbO_3$ ceramics, *J. Mater. Sci. Mater. Electron*. **30**, 2479 (2019).